Catalysis Today 157 (2010) 456–461

Contents lists available at ScienceDirect

Catalysis Today

journal homepage: www.elsevier.com/locate/cattod

Hydrogen production from ethanol in presence of water over cerium and nickel mixed oxides

L. Jalowiecki-Duhamel*, C. Pirez, M. Capron, F. Dumeignil, E. Payen

UCCS Unité de Catalyse et de Chimie du Solide, UMR CNRS 8181, Bât. C3, Université des Sciences et Technologies de Lille, 59655 Villeneuve d'Ascq Cedex, France

ARTICLE INFO

Keywords:
Hydrogen production
Ethanol
Anionic vacancies
Oxyhydrides
Nickel oxide
Ceria

ABSTRACT

Hydrogen production from ethanol in the presence of water ($H_2O/C_2H_5OH = 3$) was investigated over cerium nickel $CeNi_xO_y$ ($0 < x \leq 5$) mixed oxide catalysts. The influence of different parameters was analysed, such as reaction temperature, Ni content and *in situ* pre-treatment in H_2. While an ethanol conversion of 100% is reached at 400 °C, a stable activity i.e. ethanol conversion and H_2 selectivity can be obtained at very low temperature (200 °C) when the solid is previously *in situ* treated in H_2 in a temperature range between 200 and 300 °C. After such a treatment, the solids studied are hydrogen reservoirs, called oxyhydrides, with the presence of hydrogen species of hydride nature in the anionic vacancies of the solid. Different physicochemical techniques were used to characterize the catalysts. Depending on the composition and metal loading, a solid solution and/or a highly dispersed nickel oxide in ceria can be obtained. Correlations among the species present in the solid, and the catalytic performances are discussed, an active site based on the formation of anionic vacancies and a mechanism involving a heterolytic abstraction of a hydride species from ethanol are proposed.

1. Introduction

The potential benefits of a hydrogen economy coming from renewable energy sources are creating a large consensus [1]. Hydrogen has to be produced, and among renewable sources bio-ethanol is a promising candidate since it is readily produced from fermentation of biomass and has reasonably high hydrogen content [2–10]. In theory, hydrogen production from biomass or biomass derived liquids can be a carbon-emission free process since all carbon dioxide produced can be recycled back to plants using solar energy. Besides, ethanol is also safe, simple to handle, transport and store, so ethanol lends itself very well to a distributed-production strategy.

A very interesting use of hydrogen is based on its conversion into power in fuel cell systems. The wide-spread application of fuel cells becomes closer to reality, so increased attention is focused on hydrogen production technologies [8–10]. Solid oxide fuel cells (SOFCs) are under development as energy production devices, they allow the use of carbon-monoxide resistant nickel anodes and the use of fuels different from hydrogen at the anode, in the so-called direct internal reforming SOFC [9,10]. However the high operating temperatures undergo catalytic deactivation due to sintering of nickel crystallites and carbon deposition. Hence, worldwide efforts are in progress to discover novel, more active and more stable catalysts. Performing the reaction at lower temperature than 600 °C is a challenging goal.

$$C_2H_5OH + 3H_2O \rightarrow 2CO_2 + 6H_2 \quad (1)$$

The ideal hydrogen production by ethanol steam reforming (SR) only generates CO_2 and hydrogen (Eq. (1)). However, in reality ethanol reaction occurs by a complex mechanism and product compositions are far more complicated due to the co-occurrence of multiple reactions [2]. Noble metals have shown to have significant activity at 500–600 °C range, but high cost of these metals limits their application. As a less expensive alternative, high feedstock and high activity, nickel catalysts have been widely studied [3,4,6,7,10], although this metal favours coke deposition. The major difficulty for a reforming of ethanol is the deactivation of the catalyst due to a possible carbon deposition during ethanol decomposition, particularly at high temperature. On the other hand, it is known that metal-support interaction plays an important role during the preparation step and thermal treatments, since both of them can define the properties of final catalysts: reducibility, resistance to thermal sintering of the active sites or metallic dispersion [2]. The reducibility, the catalytic activities and coking resistant behaviors of catalysts are affected by their surface and structural properties, so the methodology used in the preparation can lead to the obtainment of materials with important properties for applications in catalytic processes, such as ethanol reforming. Moreover, carbon formation can be minimized using a support

* Corresponding author. Tel.: +33 (0)3 20 33 77 35; fax: +33 (0)3 20 33 65 61.
E-mail address: louise.duhamel@univ-lille1.fr (L. Jalowiecki-Duhamel).

0920-5861/$ – see front matter © 2010 Elsevier B.V. All rights reserved.
doi:10.1016/j.cattod.2010.03.068

with good redox properties, a promoter or enhancing the strong metal-support interaction. Better catalytic performance with good stability and high hydrogen selectivity can be expected over supports with redox properties, such as CeO_2 [3–5,7,8].

Ceria, a stable fluorite-type oxide, has been studied for various reactions utilizing its particular properties, such for example, its redox properties, which can be further enhanced in the presence of a metal or metal oxide. In the laboratory, $CeNi_xO_y$ mixed oxides were largely studied because of strong interactions existing between Ni and Ce species inside the solid [11–14]. It was reported that the catalysts correspond to a solid solution with the substitution of Ni^{2+} ions in the CeO_2 lattice when $x \leq 0.5$ and when $x > 0.5$ to compounds in which crystallized NiO and solid solution can coexist. The size of nickel oxide varies considerably from clusters to a crystallized material depending on the x value and the experimental conditions (preparation conditions, calcination temperature, etc.). Furthermore, depth sputtering followed by XPS analysis evidenced on $CeNi_{0.5}O_y$, depending on whether the solid solution is, or is not, taken into account, small particles of NiO estimated between 3.1 and 3.6 nm [13]. A series of reactions were proposed accounting for the reduction mechanism that take place in the solid solution. Redox processes between Ce^{4+}, Ce^{3+}, Ni^0 and Ni^{2+} were demonstrated. These Ni species present the characteristic of being able to be reduced and reoxidized easily and reversibly allowed by their close interaction with Ce species. Moreover, in the partially reduced state anionic vacancies able to receive hydrogen, in a hydride form, are created at the surface and in the bulk of the solid and a reduction mechanism based on heterolytic dissociation of H_2 was proposed ($O^{2-} + \square + H_2 \rightarrow OH^- + H^-$ with $\square$: anionic vacancy). Relation between the ability of the partially reduced solids for storing hydrogen, the nature of the occluded hydrogen species, and the degree of reduction of the cations was discussed [11–15]. It appears that different kinds of active sites which differ from each other in terms of the environment of Ni species can exist [16].

In the present study, we report on H_2 formation activity over $CeNi_xO_y$ catalysts from ethanol in the presence of water. The aim of this work was to develop a highly active, selective, stable and cost effective catalyst at relatively low temperature which should avoid carbon formation and also allow an application to fuel cells.

2. Experimental methods

The mixed oxides denoted $CeNi_xO_y$, where x is the Ni/Ce atomic ratio were prepared by coprecipitation of the corresponding hydroxides from mixtures of cerium and nickel nitrates (0.5 M) using triethylamine (TEA) as a precipitating agent. After filtration, the solids were dried at 100 °C and calcined in air at 500 °C for 4 h. The metal concentration M_T is the sum of Ce and Ni and $Ni/M_T = x/(1+x)$. The loading was measured by microanalysis (Centre d'analyses CNRS Vernaison). The surface areas were determined by the BET method.

Catalytic performances were conducted at atmospheric pressure with a quartz fixed-bed reactor (inner diameter 10 mm) fitted in a programmable oven, in the temperature range of 50–480 °C. When noted, the catalyst was previously *in situ* treated in H_2 at 200 °C for 10 h. The water:ethanol mixture (molar ratio 3:1) is pumped into a heated chamber and vaporized. The water–ethanol gas (N_2) stream (total flow: 60 mL/min) is then fed to the reactor containing 0.2 g of catalyst sandwiched between layers of SiC. The gases at the outlet of the reactor were taken out intermittently with the aid of a sampler directly connected to the system and analysed on-line by FID and TCD gas chromatography. Reaction data were collected as a function of time and reported after about 5 h when the steady state was obtained for each temperature. Carbon is also formed but the quantity was not analysed. The concentrations of the outlet products were calculated by excluding water, that is, dry-based gas composition.

X-ray powder diffraction (XRD) analysis was carried out with a D 5000 Siemens diffractometer using a copper target and a secondary beam monochromator. The XRD patterns were registered in the 2θ domain (15–80°) with a measured step of 0.02° and the time of integration was fixed to 12 s. The crystallites size was calculated using the Scherrer equation, from the most intense reflections observed for the NiO and CeO_2 crystallographic structures: (1 1 1), (2 0 0), (2 2 0).

Temperature-programmed reduction (TPR) was performed on a Micromeritics Autochem 2920 analyser, and hydrogen consumption was measured by a TCD detector: 25 mg of the sample was treated in the 5% H_2–95% Ar gas mixture (2 l h). The temperature was increased to 800 °C at a heating rate of 10 °C/min.

The X-ray photoelectron spectroscopy (XPS) spectra of the samples were obtained on a VG Escalab 220 XL instrument using Al Kα radiation ($h\nu$ = 1486.6 eV). The details of the spectrometer and the experimental procedure are given in Ref. [13]. The anode was operated at a power of 300 W and the fixed retardation ratio (FRR) was applied. The base pressure attained during the analysis was 1.33×10^{-6} Pa. The calcined samples were lightly pressed on an Au-holder. The measurements were performed at room temperature. For calibration of the binding energy (E_B) scale of photoemission features, the Ce3d u‴ peak at 916.7 eV was taken as an internal reference. In our experimental conditions, the reproducibility of E_B was estimated at ±0.2 eV. As for atomic ratios, they were calculated by assuming a homogeneous distribution of the catalyst components. The spectrometer allows ions to be bombarded directly onto the surface of compounds. For this, the solids were thinly pressed on an indium-holder and measurements were performed with the same analysis conditions as those previously described.

3. Results and discussion

3.1. XRD

Fig. 1 reports the diffraction patterns obtained with different $CeNi_xO_y$ solids. A ceria like phase is apparent in every solid analysed (34-0394 JCPDS file) while crystallized NiO (4-0835 JCPDS file) appears when $x \geq 0.4$. As already reported in previous studies for $CeNi_xO_y$ compounds, a careful examination of the patterns shows that the addition of nickel affects not only the broadness of the ceria peaks, but also their position, attributed to the substitution of Ce^{4+} cations by Ni^{2+} cations inside the CeO_2 lattice and interpreted by the formation of a cerium–nickel solid solution [14]. As a matter of fact, the nickel ionic radius (Ni^{2+}: 0.07 nm) is smaller than the cerium ionic radius (Ce^{4+}: 0.09 nm). It was reported that

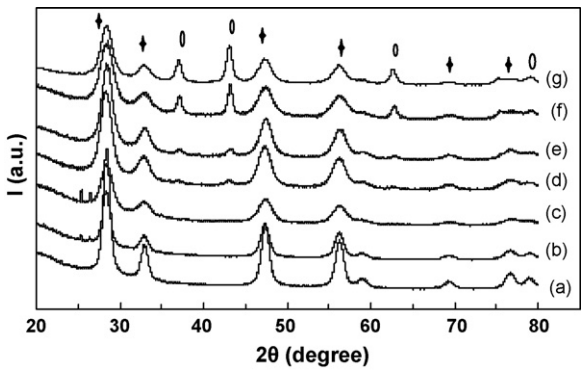

Fig. 1. XRD patterns of $CeNi_xO_y$ compounds. x = (a) 0, (b) 0.01, (c) 0.1, (d) 0.4, (e) 0.5, (f) 0.9 and (g) 2.3. CeO_2 (✦), NiO (○).

Table 1
Surface area (BET) and crystallite size (calculated from the Scherrer equation).

Catalyst	Area ($m^2\ g^{-1}$)	CeO_2 (nm)	NiO (nm)
$CeNi_{0.07}O_y$	92	5.6	–
$CeNi_{0.2}O_y$	100	5.1	–
$CeNi_{0.4}O_y$	136	4.7	8.0
$CeNi_{0.7}O_y$	91	4.8	12.0
$CeNi_{0.9}O_y$	109	4.4	11.0
$CeNi_5O_y$	84	4.6	9.4

the highest proportion of solid solution is obtained for the $CeNi_{0.5}O_y$ compound, as also observed here, when the molar ratio $Ni/M_T = 0.33$ (M_T = Ni + Ce, $Ni/M_T = x/(1+x)$). The studied $CeNi_xO_y$ mixed oxides with $x < 0.4$ correspond to a solid solution with the substitution of Ni^{2+} ions in the CeO_2 lattice, to compounds in which crystallized NiO and solid solution coexist when $0.4 \leq x < 1$, and to a mixture of CeO_2 and NiO when $x > 1$.

It was reported that the size of nickel oxide particles varies considerably from clusters to a crystallized material depending on the x value and the experimental conditions (preparation conditions, calcination temperature, etc.) [11–15]. In a similar manner as reported previously, the crystallite size was estimated from the XRD line widths taking into account the (1 1 1), (2 0 0) and (2 2 0) peaks, for both NiO and CeO_2. The average dimensions obtained for $CeNi_xO_y$ oxides are summarized in Table 1. The size of the crystallites of the mixed oxides is found smaller than the size measured for the pure oxides. This phenomenon was already explained by an increase of the crystallographic disorder in the mixed oxides. This technique allows an estimation of the average crystallites size at about 5 nm for CeO_2-like species and at about 10 nm for NiO species. However, it is important to recall that crystallites with a size smaller than 2 nm cannot be detected by XRD (because of the limits of detection).

3.2. XPS

As for the $CeNi_xO_y$ solids already studied by this technique in the laboratory [13], one can unambiguously ascribe the 3d envelope to Ce^{4+} cations in CeO_2-like species. O1s lines of the compounds have all binding energies of 529.1 ± 0.1 eV, showing without doubt that the oxygen element is characteristic of some typical O^{2-} lattice oxygen species. Moreover, a careful examination of the $Ni2p_{3/2}$ band shapes of the mixed oxides shows a line broadening effect when the nickel content increases. As already published in previous works on cerium based compounds, it can be admitted that Ni^{2+} species mainly form a solid solution with ceria for low Ni contents. For high Ni/Ce ratios several types of surface nickel seem to coexist, in agreement with XRD. Therefore, the system can be described as a solid solution of nickel in ceria in close contact with nickel oxide.

However, some quantitative XPS features provide additional information. Superficial nickel compositions of the mixed oxides determined from XPS atomic ratios are compared to bulk nickel content (elemental analysis) in Fig. 2. The 45° diagonal line corresponds to the case of a homogeneous distribution of nickel inside the solid, and rather good results are obtained on the studied compounds when comparing with the results obtained on a precedent series of catalysts [17].

Ions sputtering in combination with surface analysis techniques such as XPS provide information on the in-depth distribution of elements inside the solid. This technique found many applications in materials that show some composition inhomogeneity in their topmost layers and was previously detailed and applied in our laboratory to characterize the $CeNi_xO_y$ compounds [13]. During the first minutes of sputtering, there is a sharp decrease of the Ni/Ce ratio, registered on all the binary oxides, confirming that the structure does not correspond to a homogeneous solid solution, the presence of small particles in strong interaction with some bigger particles can be in such a case privileged, whatever the nickel content included in the $CeNi_xO_y$ compounds. In order to estimate the size of the NiO particles on the support, two models were suggested, allowing simplifying the problem in two extreme cases, taking into account or not the presence of a solid solution of nickel in ceria. Despite the fact that these two cases describe a very simple structure of the $CeNi_xO_y$ catalysts, they allow the calculation of the particles size by default and by excess. The results obtained using these models are summarized in Table 2, showing an increase of the NiO crystallite size when the solid solution is taken into account. Therefore, as an example, the size of the NiO crystallites is respectively estimated to be 3.4 and 2.1 nm for the $CeNi_{0.5}O_y$ compound ($x = 0.5$), when taking into account or not the presence of a solid solution. However, as XRD analyses show the presence of cerium nickel solid solution for low Ni contents, the first value is more probable. Clearly some small NiO particles, smaller than the ceria particles (5 nm), coexist with larger NiO crystallites (10 nm) observed by XRD.

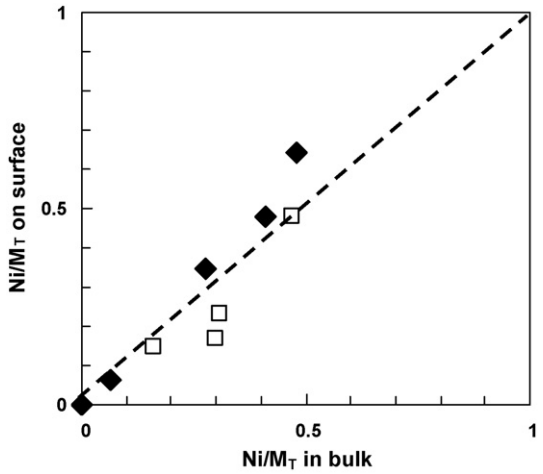

Fig. 2. Variation of Ni/M_T surface ratio (XPS) as a function of Ni/M_T bulk ratio (microanalysis) in the $CeNi_xO_y$ compounds. This work (♦) and from Ref. [18] (□).

3.3. TPR in H_2

The temperature-programmed reduction (TPR) profiles in H_2 of the catalysts are shown in Fig. 3. A first temperature reduction peak at bout 270 °C is more intense for a low Ni content, when $x = 0.1$. When x increases from 0.1 up to 0.4 a second peak at about 370 °C increases. For higher Ni contents, the first peak decreases while the second peak shifts to higher temperatures (390 °C). It was already observed that a shoulder at 440 °C is emerging in the shape of the curve obtained for higher Ni contents [17]. The reduction peak obtained at about 400 °C increases with the Ni content. For temperatures lower than 600 °C, a linear relationship is obtained between the total hydrogen consumed during TPR with the Ni content of the $CeNi_xO_y$ compounds (Fig. 4), showing that H_2 is consumed in majority to reduce nickel species in this range of temperatures. It is usually reported that TPR analysis of CeO_2 presents two peaks at about 500 and 820 °C, and that the reduction peak obtained at temperature higher than 700 °C corresponds to the reduction of

Table 2
Estimation of NiO crystallites size (nm) by depth sputtering followed by XPS for $CeNi_xO_y$ taking into account (with) or not (without) the presence of solid solution.

Solid solution	$x = 0.2$	$x = 0.5$	$x = 1$
Without	0.4	2.1	1.2
With	2.4	3.4	1.5

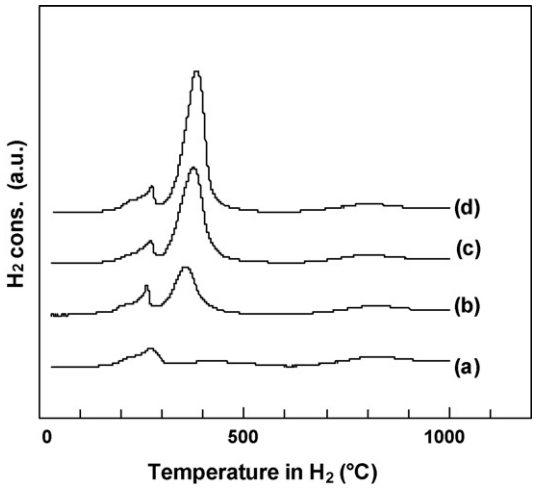

Fig. 3. TPR of $CeNi_xO_y$ compounds. x = (a) 0.07, (b) 0.4, (c) 0.7 and (d) 0.9.

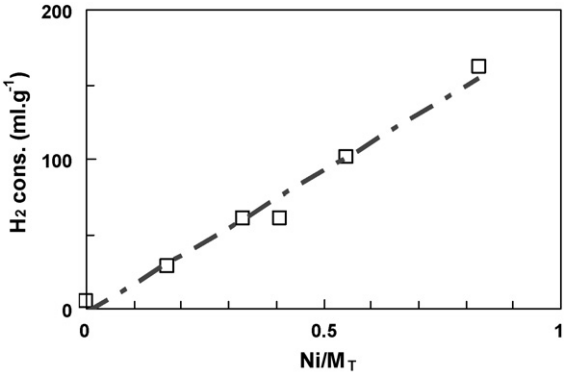

Fig. 4. H_2 consumed during TPR versus Ni content of $CeNi_xO_y$ compounds.

bulk Ce^{4+} to Ce^{3+} [18]. Moreover, it was also shown that NiO facilitates the reduction of a cerium solid solution [14,17], therefore it can be proposed that the TPR peaks correspond to the reduction of nickel species in various environments. The low temperature peak can be attributed to nickel species: (i) belonging to the solid solution and/or to (ii) small NiO particles, easily reducible, but with the simultaneous reoxidation of a part of these species by reduction of the Ce^{4+} ions in their vicinity into Ce^{3+} species as the existence of a redox system was established (Eqs. (2) and (3)), then larger NiO crystallites are reduced when increasing temperature:

$$Ni^{2+} + O^{2-} + H_2 \rightarrow Ni^0 + H_2O + \square \quad (2)$$

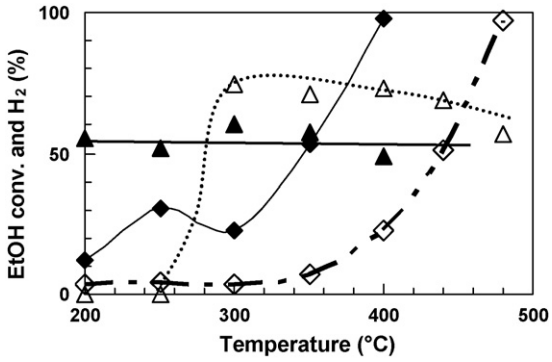

Fig. 5. Ethanol conversion (♦, ◊) and H_2 (▲, △) formation over fresh (white) and treated in H_2 at 200 °C (black) $CeNi_{0.5}O_y$ catalyst.

(with □: anionic vacancy),

$$2Ce^{4+} + Ni^0 \leftrightarrow 2Ce^{3+} + Ni^{2+} \quad (3)$$

3.4. Ethanol transformation in the presence of water

Ethanol transformation in the presence of water was studied as a function of reaction temperature, activation treatment in H_2 and metal loading of $CeNi_xO_y$ catalysts. Figs. 5 and 6 show, as examples, the results obtained over the fresh and treated in H_2 $CeNi_{0.5}O_y$ catalyst versus reaction temperature. Over the fresh catalyst, without any H_2 pre-treatment, an ethanol conversion is observed at temperatures higher than 300 °C, as expected it increases with temperature, and reaches 100% at 480 °C (Fig. 5). When the $CeNi_{0.5}O_y$ catalyst is previously *in situ* treated in H_2 at 200 °C during 10 h, there is globally an increase versus temperature but with the existence of an optimum at about 30% of conversion for a reaction temperature of 250 °C. Finally, total ethanol conversion is obtained at 480 and 400 °C over, respectively, the fresh and H_2 treated catalyst with about 50% of H_2 among the gas phase products. So total ethanol conversion with about the same H_2 yield are obtained at 80 °C lower with an adequate pre-treatment of the catalyst in H_2.

Over the treated in H_2 $CeNi_{0.5}O_y$ catalyst, the other products obtained in the outlet gas stream are acetaldehyde, CO, CH_4 and CO_2 (Fig. 6). Whatever the temperature, ethylacetate and acetone formations are lower than 0.5%. Acetaldehyde decreases with temperature (Eq. (4)) and disappears at 400 °C. CO and CH_4 present optima at 250 °C (Eq. (5)) following the evolution of conversion. For temperatures higher than 300 °C, CH_4 increases while CO remains at about 10%. Concentration of CO_2 is lower than 1% at 200 °C so as expected, the steam reforming of ethanol (Eq. (1)) is negligible at these low temperatures, and it increases for higher temperatures.

$$C_2H_5OH \rightarrow CH_3CHO + H_2 \quad (4)$$

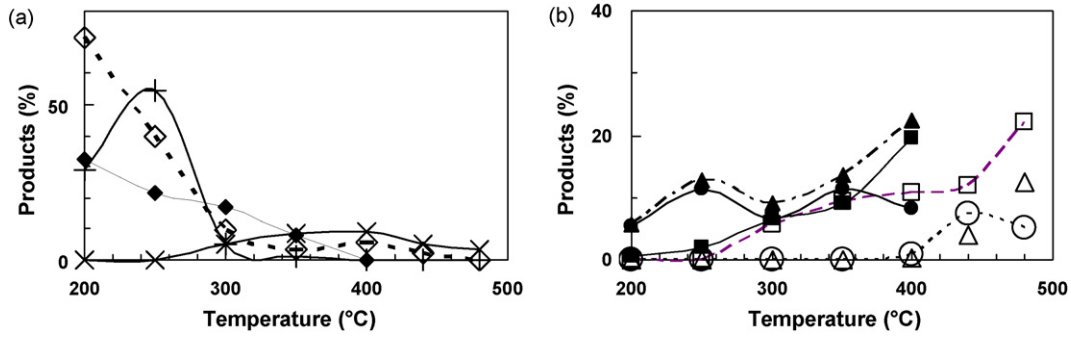

Fig. 6. Products distribution obtained over fresh (white) and treated in H_2 at 200 °C (black) $CeNi_{0.5}O_y$ catalyst. (a) Acetaldehyde (♦, ◊), ethylacetate (+) and acetone (x). (b) CO_2 (□, ■), CO (○, ●) and CH_4 (▲, △). No ethylacetate, no acetone over treated in H_2 catalyst.

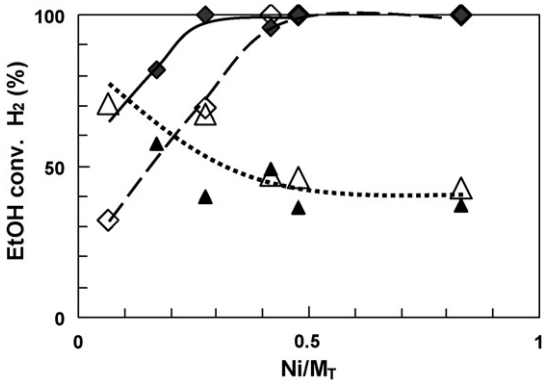

Fig. 7. Ethanol conversion (♦, ◊) and H_2 formation (▲, △) at 440 °C over fresh (white) and treated in H_2 at 200 °C (black) $CeNi_xO_y$ compounds.

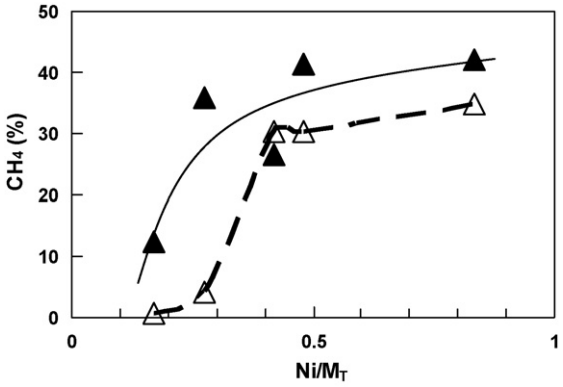

Fig. 9. CH_4 formation at 440 °C over fresh (△) and treated in H_2 at 200 °C (▲) $CeNi_xO_y$ compounds.

$$C_2H_5OH \rightarrow H_2 + CH_4 + CO \quad (5)$$

Over the fresh $CeNi_{0.5}O_y$ catalyst, between 200 and 300 °C the gas phase products observed are acetaldehyde and ethylacetate (Fig. 6a) (Eq. (6)), typical of dehydrogenation reaction (with a very low ethanol conversion ~1%), and at 300 °C, about 70% of H_2 is observed. Ethylacetate, acetaldehyde and acetone are found in concentration range between 5 and 10% depending on the reaction temperature. For temperatures higher than 300 °C ethylacetate disappears, while acetone appears at 300 °C (Eq. (7)) and presents an optimum of 10% at about 400 °C. CO_2 appears at temperatures higher than 250 °C and increases with temperature, while CO and CH_4 are formed at temperatures higher than 400 °C (Eq. (5)).

$$CH_3CHO + C_2H_5OH \rightarrow CH_3COOC_2H_5 + H_2 \quad (6)$$

$$2CH_3CHO + H_2O \rightarrow CH_3COCH_3 + 2H_2 + CO_2 \quad (7)$$

The catalytic results obtained depend on the Ni content of the compounds, in particular for ethanol conversion. At 440 °C ethanol conversion increases with Ni content and is of 100% when $Ni/M_T \geq 0.4$ ($CeNi_{0.7}O_y$) over fresh catalysts and when $Ni/M_T \geq 0.3$ over treated in H_2 catalysts (Fig. 7), while H_2 formation decreases from about 70% to about 40% when increasing the Ni/M_T ratio almost whatever fresh or H_2 treated catalysts. The products distribution depends on the ethanol conversion, and even if the selectivities should be compared for similar conversions, one can remark some tendencies. Acetone is formed only over fresh compounds for low Ni contents and it disappears when $Ni/M_T \geq 0.4$ (Fig. 8) when conversion is total. Acetaldehyde is formed over compounds with low Ni contents and favoured over fresh catalysts. Therefore, at 440 °C oxygenated compounds formation (other than CO_x) are favoured over fresh catalysts and low Ni contents, with the lowest conversions. As shown in Fig. 9, CH_4 formation is higher over the H_2 treated compounds and with high Ni contents. CO is favoured over low Ni content H_2 treated catalysts (Fig. 10) and disappears at high Ni contents with total conversion due to water gas shift reaction. CO_2 and CH_4 follow almost similar evolutions over treated and not treated catalysts with an increase with Ni content, following total conversion (Figs. 9 and 10). Finally, at 440 °C over the treated in H_2 $CeNi_{0.7}O_y$ catalyst ($Ni/M_T = 0.4$), only H_2, CH_4, CO and CO_2 gases are obtained with a very low amount of CO. It is important to recall that solid carbon is also formed, and in relatively high quantity at this high temperature, but without deactivation of the catalyst. The precise analysis of carbon formation is not performed because it is not the aim of the present study, but as this parameter is also important it will be the subject of a future publication.

As the treatment in H_2 (T_T) at 200 °C leads to a dramatic effect on H_2 formation at low temperatures (≤250 °C), the influence of T_T in H_2 was studied over the $CeNi_{0.7}O_y$ chosen catalyst. As shown in Fig. 11, ethanol conversion at 250 °C presents an optimum for a treatment temperature T_T in H_2 of 275 °C, following in a quite interesting way the first reduction peak seen by TPR. Moreover, the products distribution in the outlet gas stream depends also on T_T. H_2 is formed at 250 °C with T_T higher than 100 °C. For treatment temperatures T_T in H_2 lower than 200 °C, ethylacetate is the main product obtained with acetaldehyde as by-product. Formation of H_2 is optimum over a treated in H_2 at 200 °C catalyst, but for higher treatment temperatures it remains relatively stable. CH_4 and CO concentrations follow same evolutions; they present optima for $T_T \cong 275$ °C like conversion, and when acetaldehyde concentration presents a minimum. For $T_T \geq 200$ °C, ethanol dehydrogenation to

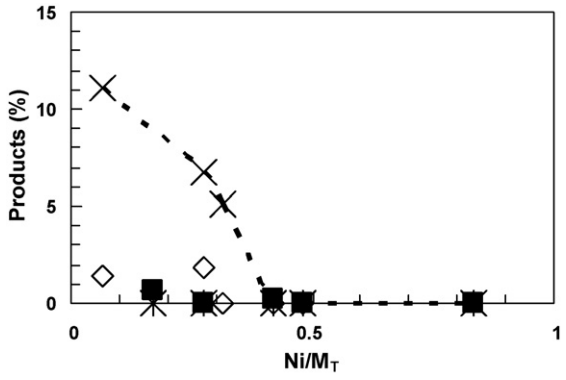

Fig. 8. Acetaldehyde (♦, ◊) and acetone (*x*) formation at 440 °C over fresh (white) and treated in H_2 at 200 °C (black) $CeNi_xO_y$ compounds. No acetone over treated in H_2 catalyst.

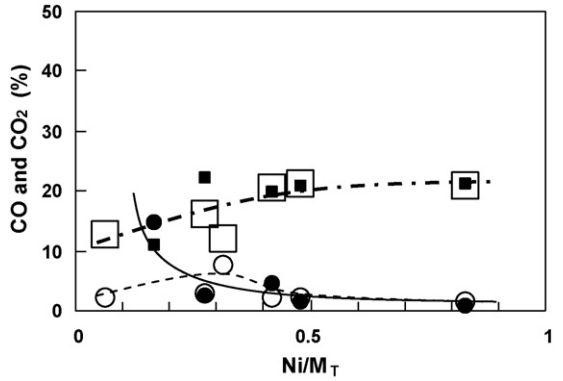

Fig. 10. CO (○, ●) and CO_2 (□, ■) formation at 440 °C over fresh (white) and treated in H_2 at 200 °C (black) $CeNi_xO_y$ compounds.

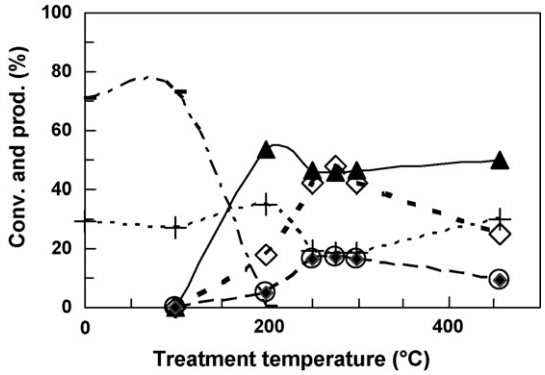

Fig. 11. Ethanol conversion (◊) and products obtained at 250 °C over $CeNi_{0.7}O_y$ catalyst versus treatment temperature in H_2. H_2 (▲) CH_3CHO (+), ethylacetate (−), CH_4 (♦) and CO (○). CO_2 (<1%).

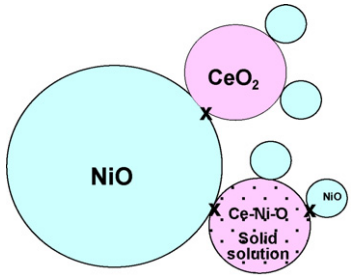

Scheme 1. Ni species in interaction with Ce species in the cerium nickel solid solution ⊙ and at the interface (*x*) between small and large NiO crystallites and CeO_2 or cerium and nickel solid solution.

acetaldehyde and ethanol decomposition reaction seem to occur as the main reactions (Eqs. (4) and (5)). The decomposition reaction (Eq. (5)) is accentuated at 250 °C when the solid is activated in H_2 between 250 and 300 °C. When the solid is activated in H_2 at $T_T > 300$ °C, decomposition reaction decreases but it is important to recall that conversion decreases too.

It is well known that physicochemical properties of a catalyst play an important role in the evolution of surface reactions. In ethanol transformation both dehydrogenation to acetaldehyde or dehydration to ethylene can occur upon the nature of the catalyst. Clearly, $CeNi_xO_y$ catalysts possess good dehydrogenation properties, accentuated once treated in H_2 at 275 °C corresponding to the first TPR peak.

Besides, after an *in situ* treatment in H_2 in particular between 200 and 300 °C, it was shown that the $CeNi_xO_y$ solids studied become hydrogen reservoirs. During the activation treatment in H_2 in temperature, the anionic vacancies created are able to accept hydride species and the solids were called oxyhydrides [14,15]. Moreover, taking into account the structure of the catalysts, particular active sites were modeled, involving anionic vacancies, hydrogen species and cations in strong interaction whatever in the solid solution or at the NiO and ceria, and/or solid solution (with Ni) interfaces, as reported as an example in Scheme 1. These sites were noted $^{x}M–^{y}M'$ and *x* and *y* correspond to the number of coordinative unsaturations i.e. anionic vacancies on each cation M and M′ [16]. Different kinds of active sites which differ from each other in terms of the environment of Ni can exist.

Therefore, H_2 production from ethanol in the presence of water certainly involves particular Ni species in strong interaction with Ce species. These Ni species are easily reducible and reoxidable by the presence of Ce in close vicinity (redox system). Clearly, the treatment in H_2 between 200 and 300 °C leads to a beneficial effect on H_2 production. It was shown that this treatment allows the $CeNi_xO_y$ mixed oxides to accept large quantities of hydrogen by the presence of anionic vacancies. Therefore, over the fresh catalyst, up to 300 °C acetaldehyde and ethylacetate are observed and H_2 produced from ethanol is certainly consumed by the solid leading to a partially reduced compound. Taking into account that dehydrogenation step requires abstraction of hydrogen species from alcohol, the ability of the solid to accept hydrogen can be a prerequisite condition and "filling" the solid with hydrogen (during the pre-treatment in H_2) allows its formation from alcohol at low temperatures. Therefore, by analogy to heterolytic dissociation of H_2, heterolytic dissociation of ethanol can be envisaged on a low coordination site involving an anionic vacancy, as it was already proposed for oxidative dehydrogenation of propane [19] and methane activation [17] over $CeNi_xO_y$ compounds.

4. Conclusion

Ethanol transformation in the presence of water was studied over $CeNi_xO_y$ ($0 < x \leq 5$) catalysts. The active nickel species belongs to the NiO nano-particles and/or to the cerium nickel solid solution where Ni species are in strong interaction with Ce species. Hydrogen can be produced at low temperature ≤250 °C once the $CeNi_xO_y$ mixed oxides are previously *in situ* treated in H_2 at about 250 °C leading to the formation of oxyhydrides. Therefore, an active site is proposed based on the presence of anionic vacancies able to abstract hydride species from ethanol.

Acknowledgements

One of the authors gratefully acknowledge for a grant from French Ministry. The authors would like to thank the CE for its financial support through the contract number MIRG-CT-2007-046383.

References

[1] M. Momirlan, T.N. Veziroglu, Int. J. Hydrogen Energy 30 (2005) 795.
[2] M. Ni, D.Y.C. Leung, M.K.H. Leung, Int. J. Hydrogen Energy 32 (2007) 3238.
[3] P. Biswas, D. Kunzru, Int. J. Hydrogen Energy 32 (2007) 969.
[4] F. Romeiro-Sarria, J.C. Vargas, A.C. Roger, A. Kiennemann, Catal. Today 133 (2008) 149.
[5] W.J. Cai, F.G. Wang, E.S. Zhan, A.C. Van Veen, C. Mirodatos, W.J. Shen, J. Catal. 257 (2008) 96.
[6] F. Wang, Y. Li, W. Cai, E. Zhan, X. Mu, W. Shen, Catal. Today 146 (2009) 31.
[7] H.V. Fajardo, L.F.D. Probst, N.L.V. Carreño, I.T.S. Garcia, A. Valentini, Catal. Lett. 119 (2007) 228.
[8] S.M. de Lima, R.C. Colman, G. Jacobs, B.H. Davis, K.R. Souza, A.F.F. de Lima, L.G. Appel, L.V. Mattos, F.B. Noronha, Catal. Today 146 (2009) 110.
[9] L.E. Arteaga, L.M. Peralta, V. Kafarov, Y. Casas, E. Gonzales, J. Chem. Eng. 136 (2008) 256.
[10] C. Resini, M.C.H. Delgado, S. Presto, L.J. Alemany, P. Riani, R. Marazza, G. Ramis, G. Busca, Int. J. Hydrogen Energy 33 (2008) 3728.
[11] G. Wrobel, M.P. Sohier, A. D'Huysser, J.P. Bonnelle, J.P. Marcq, Appl. Catal. 101 (1993) 73.
[12] G. Wrobel, C. Lamonier, A. Bennani, A. D'Huysser, A. Aboukaïs, J. Chem. Soc. Faraday Trans. 92 (1996) 2001.
[13] A. Ponchel, A. D'Huysser, C. Lamonier, L. Jalowiecki-Duhamel, Phys. Chem. Chem. Phys. 2 (2000) 303.
[14] C. Lamonier, A. Ponchel, A. D'Huysser, L. Jalowiecki-Duhamel, Catal. Today 50 (1999) 247.
[15] L. Jalowiecki-Duhamel, A. Ponchel, C. Lamonier, Int. J. Hydrogen Energy 24 (1999) 1083.
[16] L. Jalowiecki-Duhamel, Int. J. Hydrogen Energy 31 (2006) 191.
[17] L. Jalowiecki-Duhamel, H. Zarrou, A. D'Huysser, Int. J. Hydrogen Energy 33 (2008) 5527.
[18] P. Fornasiero, R. Di Monte, G.R. Rao, J. Kaspar, S. Meriani, A. Trovarelli, M. Graziani, J. Catal. 151 (1995) 168.
[19] L. Jalowiecki- Duhamel, A. Ponchel, C. Lamonier, A. D'Huysser, Y. Barbaux, Langmuir 17 (2001) 1511.